small methods
www.small-methods.com

TiN-Au/HfO_2-Au Multilayer Thin Films with Tunable Hyperbolic Optical Response

*Yizhi Zhang, Jianan Shen, Benson Kunhung Tsai, Xuanyu Sheng, Zedong Hu, Xinghang Zhang, and Haiyan Wang**

Hyperbolic metamaterials (HMM) possess significant anisotropic physical properties and tunability and thus find many applications in integrated photonic devices. HMMs consisting of metal and dielectric phases in either multilayer or vertically aligned nanocomposites (VAN) form are demonstrated with different hyperbolic properties. Herein, self-assembled HfO_2-Au/TiN-Au multilayer thin films, combining both the multilayer and VAN designs, are demonstrated. Specifically, Au nanopillars embedded in HfO_2 and TiN layers forming the alternative layers of HfO_2-Au VAN and TiN-Au VAN. The HfO_2 and TiN layer thickness is carefully controlled by varying laser pulses during pulsed laser deposition (PLD). Interestingly, tunable anisotropic physical properties can be achieved by adjusting the bi-layer thickness and the number of the bi-layers. Type II optical hyperbolic dispersion can be obtained from high layer thickness structure (e.g., 20 nm), while it can be transformed into Type I optical hyperbolic dispersion by reducing the thickness to a proper value (e.g., 4 nm). This new nanoscale hybrid metamaterial structure with the three-phase VAN design shows great potential for tailorable optical components in future integrated devices.

1. Introduction

Hyperbolic metamaterials (HMMs) have recently attracted great research interest because of their wide range of applications in optics and photonic devices, such as negative refraction,[1–3] hyperlens,[4,5] and partial focusing.[6,7] In the hyperbolic metamaterials, the signs of the permittivity along different directions are opposite, leading to the hyperbolic physical response.[8] Typically, the hyperbolic metamaterials consist of metal and dielectric materials arranged in highly anisotropic morphology.[9]

In general, there are multiple approaches to produce such hyperbolic metamaterials. One is alternative deposition of metal and dielectric material as multilayers, such as TiN/MgO multilayers, Ag/SiO_2 multilayers, TiN/AlN multilayers, and TiN/ScN multilayers.[10–14] Another one is to use top-down lithography and patterning methods, such as focused ion beam and e-beam lithography, to prepare highly anisotropic metal-dielectric nanostructures.[15–17] The vertically aligned nanoarrays structure can also be achieved by chemical synthesis methods, such as electrodeposition, vacuum-filtration technique and kinetic assembly method.[18–20] Very recently, a one-step deposition of self-assembled oxide-metal metamaterials in a vertically aligned nanocomposites (VANs) form has been demonstrated as an alternative approach for processing HMMs.[18,19,21,22]

Considering different responses, hyperbolic metamaterials can be mainly divided into two different types, as shown in the schematic drawing in **Figure 1**.[9] In the Type I hyperbolic metamaterials, in-plane ($\epsilon^{//}$) dielectric constant real part is positive, while out-of-plane ($\epsilon^{\perp}$) is negative. Such Type I hyperbolic dispersion can usually be achieved in some metal in dielectric VAN structure.[9,21,23,24] On the contrast, in the Type II hyperbolic metamaterials, n-plane ($\epsilon^{//}$) dielectric constant real part is negative, while out-of-plane ($\epsilon^{\perp}$) is positive. Such Type II hyperbolic dispersion has been reported in some metal dielectric multilayer structures.[10,12,25,26] Thus it is hypothesized that tunable hyperbolic metamaterials could be achieved by combining two different structure designs, i.e. VAN and multilayers. Such combined multilayers and VAN structures have been very rarely explored with limited success[27] but could have a great potential in achieving tunable hyperbolic metamaterials.

As alternative plasmonic materials to noble metals, transition metal nitrides have been recently explored to produce metal/dielectric multilayer HMMs, owing to their high hardness and stability, low cost, and excellent plasmonic properties in the wavelength range from 500 to 600 nm.[10,12] As a typical transition metal nitride, TiN has been widely studied to fabricate

Y. Zhang, J. Shen, B. K. Tsai, X. Sheng, X. Zhang, H. Wang
School of Materials Engineering
Purdue University
West Lafayette, IN 47907, USA
E-mail: hwang00@purdue.edu
Z. Hu, H. Wang
School of Electrical and Computer Engineering
Purdue University
West Lafayette, IN 47907, USA

The ORCID identification number(s) for the author(s) of this article can be found under https://doi.org/10.1002/smtd.202400087

DOI: 10.1002/smtd.202400087

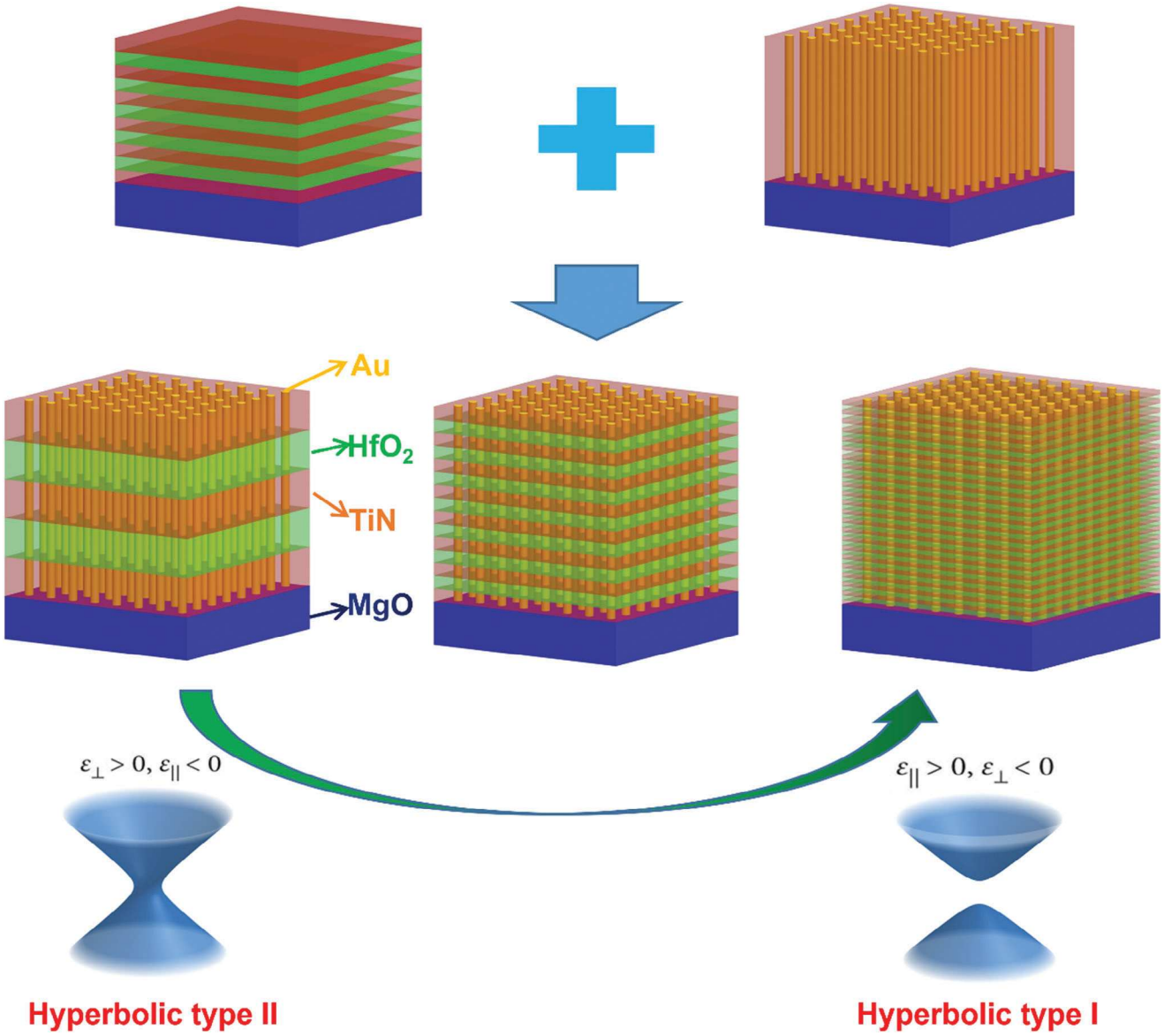

Figure 1. Schematic drawing of the new multilayers structure design, leading to the hyperbolic dispersion transformation from Type II to Type I when layer thickness decreases.

HMMs as the metallic phase in the form of either nanoarrays or multilayers.[10,12,28,29] TiN displays unique optical properties as a plasmonic, and possess high stability with a high melting point.[30,31] However, TiN has been reported to be oxidized over 400 °C,[32,33] which makes it challenging to integrate TiN with oxide to produce HMMs. In addition, the growth conditions for most oxides and nitrides are different which also poses a growth challenge.

In this work, we demonstrated a new anisotropic structure design combining both multilayer and VAN structures, where TiN-Au and HfO_2-Au were alternatively deposited on MgO substrate with a PLD method, to fabricate tunable HMMs. HfO_2 was selected as the dielectric material, because our previous study reveals that the epitaxial HfO_2-Au layer can be obtained on a TiN-Au layer by the direct deposition of HfN-Au.[21] In the previous work, we found that the Au pillars can grow vertically in both TiN and HfO_2 layers, and detailed TEM analysis shows that the Au pillars can grow continuously through the interface between TiN and HfO_2. In addition, the work also reveals that the TiN was not oxidized under such vacuum growth condition. We thus hypothesize that the HfN oxidation process could also help mitigate the oxidation process of TiN. This phenomenon makes it possible to fabricate such HfO_2-Au/TiN-Au multilayers structure without much concern of the oxidation of TiN. The layer thickness was varied by adjusting laser pulses for each individual layer while controlling the total film thickness, as shown in Figure 1. This has resulted in different layer numbers of 5, 15, and 45 for the three samples. Optical measurements were conducted to explore the optical property tuning in this complex 3-phase nanocomposite system. The work provides additional tuning approaches in

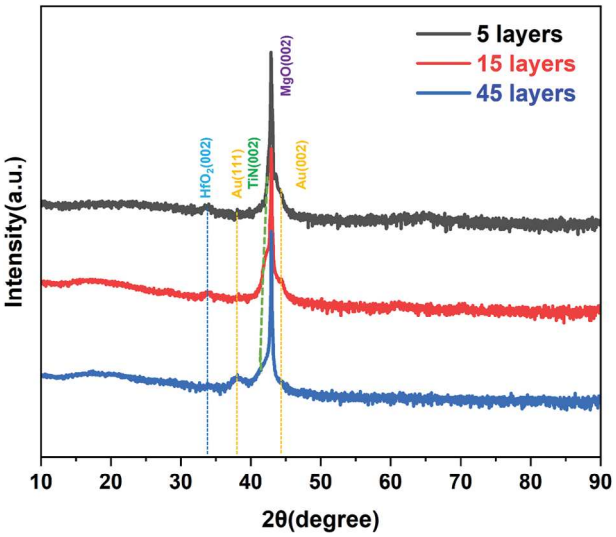

Figure 2. XRD θ-2θ scan of HfO_2-Au/TiN-Au multilayers with different layer thickness.

plasmonic HMMs designs towards future applications in integrated photonic structures.

2. Results and Discussion

Three TiN-Au/HfO_2-Au multilayer samples (i.e., 5 layers, 15 layers, and 45 layers) were deposited on MgO substrate considering the lattice matching between MgO (a = 4.21 Å) and TiN (a = 4.24 Å). Both top layers and bottom layers are TiN layers. To investigate the overall film crystallinity, the X-ray diffraction (XRD) characterization was conducted on all three as-deposited films, and the results are shown in **Figure 2**. Both monoclinic-HfO_2 (002) peaks and cubic-TiN (002) peaks can be distinguished at $\approx 2\theta$ = 34.3 and 2θ = 42.5 respectively. Neither TiO_2 nor TiNO peaks can be identified suggesting no obvious oxidation of TiN was found in the samples. It is worth noting that the peak intensity of both HfO_2 (002) and TiN (002) peaks decreases as the layer number increases, suggesting the film crystallinity was reduced as each layer becomes thinner. This is perhaps due to the in-plane lattice mismatch between TiN (a = 4.24 Å) and HfO_2 (a = 5.09 Å, b = 5.15 Å, c = 5.28 Å) and there is more in-plane strain in the thinner layer samples. It can also be noted that the Au prefers (002) orientated growth in the 5-layers film, and it became (111) dominated in the 45-layers film. This orientation difference could be related to the film crystallinity and strain state in the samples.

The specific film morphology analysis was conducted using STEM and EDS, and results are shown in **Figure 3**. In the STEM images taken under the high angle annular dark field (HAADF) mode, two different layers can be easily distinguished based on the contrast, i.e. the darker layers are TiN, and the brighter layers are HfO_2. It can be observed that the layer thickness in all three films is almost uniform, and thickness of TiN layer is comparable to that of HfO_2 layer. In the 5-layer film, each layer is ≈20 nm, while that is 12 nm in the 15-layer film and 4 nm in the 45-layer film. In the meantime, the Au pillars can grow through all the films in a vertical direction with fairly uniform size. There are some curvature and diameter variation when Au pillars grow through different layers, and the average diameter of the Au pillars was measured to be ≈3.5 nm in all three films. The diameter variation in different layers can be resulted from the strain difference in each of the matrix layers. The corresponding selected area electron diffraction (SAED) patterns for all samples are shown in Figure S1 (Supporting Information). The corresponding selected area electron diffraction (SAED) patterns for all samples are shown in Figure S1 (Supporting Information). In the diffraction pattern of the 5-layer film, all diffraction spots are clear and sharp, suggesting a high-quality epitaxial growth. Both TiN and HfO_2 diffraction spots can be easily distinguished. However, the diffraction patterns suggest that the films become polycrystalline and amorphous in some areas as the layer number increases, indicating a reduced crystallinity. This result agrees well with the XRD results.

The volume fill fraction of Au pillars was also estimated from the microscope images. The plan-view (PV) imaging analysis was conducted on these multilayer samples to help with the estimation, and the relative EDS mapping are shown in the Figure S2 (Supporting Information). It can be observed that all three samples have a similar distribution of the Au pillars, and the average distance between Au pillars is similar for all three samples to be ≈7 nm. The big difference of the pillars size in PV EDS images could result from the sample preparation process due to curvature and diameter variation of pillars. The average pillar size in cross-sectional (CS) image and pillar distribution in PV image were used to estimate the volume fill fraction. In this estimation, the Au pillars are regarded as the cylinder with the diameter of 3.5 nm. And the pillar amount density is calculated to be 0.0188, 0.0197, and 0.0175 nm^{-2} accordingly. Then the volume fill fraction was estimated to be ≈18.1% (5 layers), 19.1% (15 layers), and 16.8% (45 layers).

To better understand the interface and crystallinity, the 5-layer film was selected to perform more detailed microstructure analysis. The TEM image and corresponding SAED patterns are shown in **Figure** 4a,b, respectively. TiN and HfO_2 layers can be easily recognized with different contrast. By carefully indexing the diffraction patterns, cubic TiN and monoclinic HfO_2 with different orientations can be distinguished. Since the lattice parameters of TiN and MgO are comparable, some of their diffraction spots are overlapped. However, there are some other diffraction spots not indexed in the figure, which are identified as Au diffraction spots. The distinguished diffraction pattern indicates nearly epitaxial growth of TiN and HfO_2 multilayers, with the epitaxial relation of HfO_2(002)//TiN(002), which is consistent with the XRD results. Further interface analysis was performed with HRSTEM and shown in Figure 4c,d. It can be observed that the interfaces between TiN and HfO_2 are smooth, and local high-resolution STEM image further confirms that the HfO_2 is in monoclinic structure and TiN is in cubic structure without oxidation. Based on the HRSTEM image, Au pillars grow continuously through the interface between TiN and HfO_2, marked with yellow dash line in Figure 4d. The average Au nanopillar diameter can be estimated to be ≈3.5 nm, which is relatively thin compared to previously reported Au pillars in VAN structures.[34–36]

To investigate the optical properties of such anisotropic structures, ellipsometry measurement was performed on all three films by RC2. Based on the (S)TEM results, the x-direction and y-direction performance should be equivalent, so the obtained

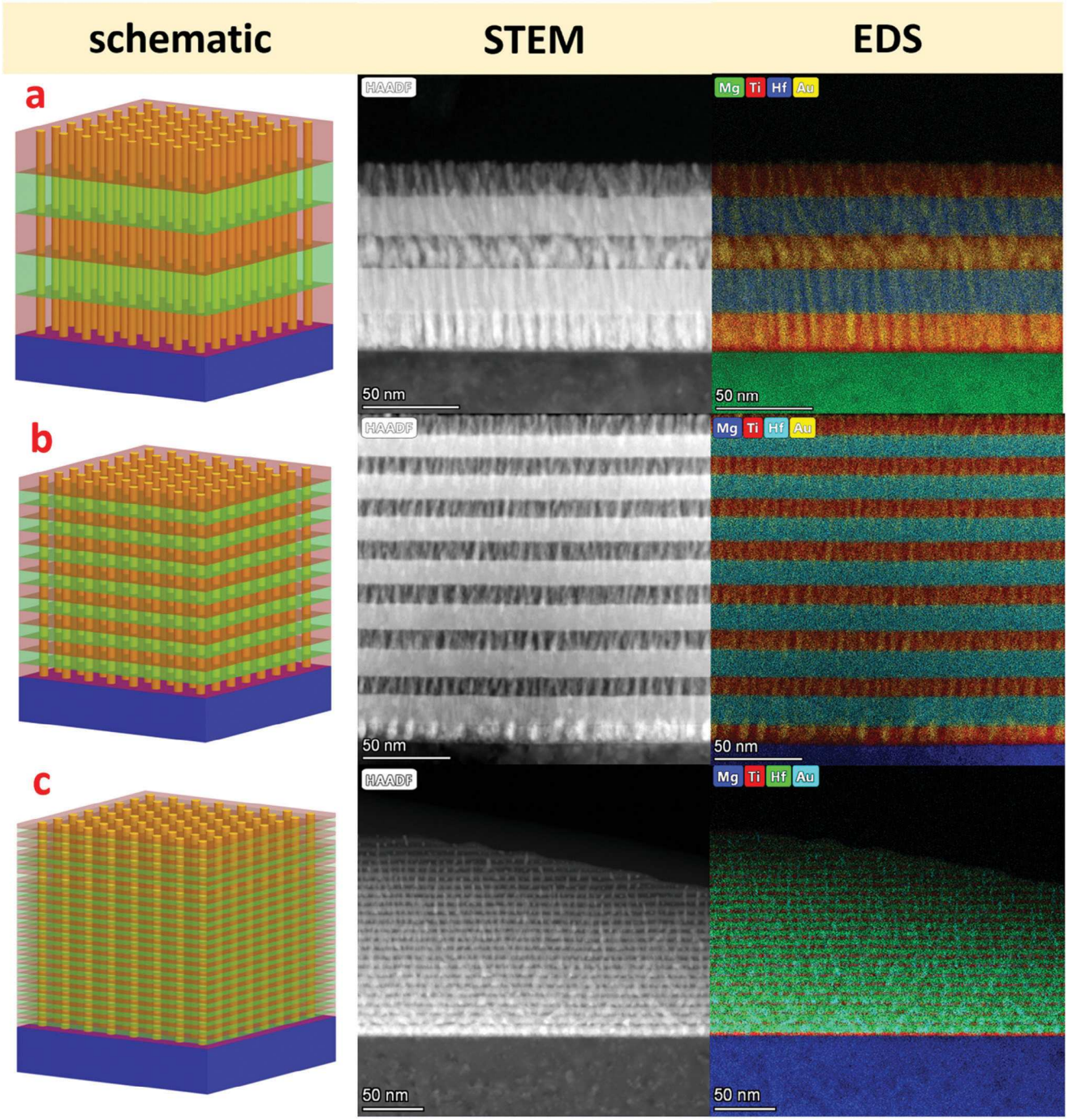

Figure 3. STEM images and EDS mappings of HfO_2-Au/TiN-Au multilayer films with different numbers of layers: (a) 5 layers, (b) 15 layers, and (c) 45 layers.

data was fitted with biaxial model along with general oscillator, and the results were plotted in **Figure 5**. Remarkably, different optical hyperbolic dispersion properties can be obtained in the three samples with a general trend. Figure 5a suggested that for wavelengths less than 630 nm in the 5-layers film, both in-plane ($\epsilon^{//}$) and out-of-plane ($\epsilon^{\perp}$) dielectric constant real part are positive, while $\epsilon^{//}$ turns into negative and $\epsilon^{\perp}$ remains positive above 630 nm, leading to the Type II hyperbolic dispersion. This result is similar to that of the most reported multilayer hyperbolic metamaterials, which exhibit Type II hyperbolic dispersion above specific wavelength.[10,12,25,26] Especially for TiN-based hyperbolic metamaterials, TiN/AlN multilayers have been widely explored and previous research has reported that Type II hyperbolic dispersion can be obtained beyond 600 nm in such TiN based multilayer hyperbolic metamaterials.[12,25]

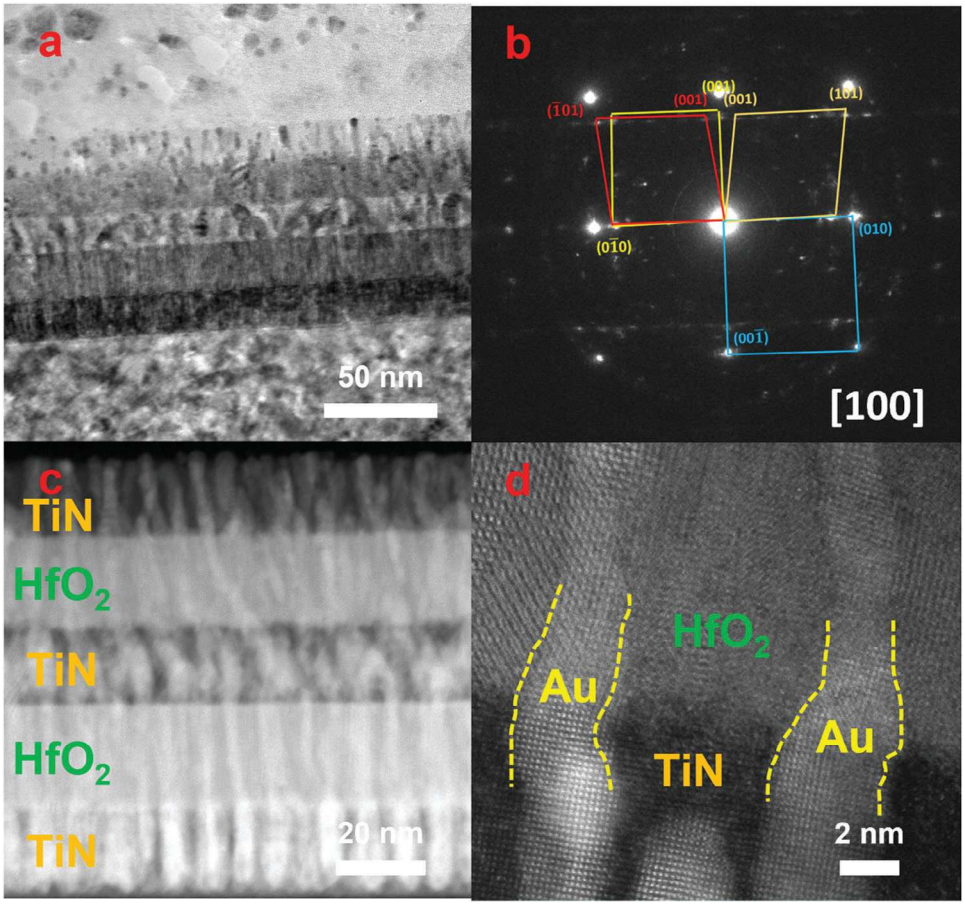

Figure 4. Microstructure analysis of the 5-layers HfO_2-Au/TiN-Au multilayer thin film. (a) TEM image, (b) the corresponding selected area diffraction pattern obtained under the zone axis [100], (c) STEM and (d) HRSTEM images of the interface between HfO_2 layer and TiN layer. In the diffraction pattern, the blue mark is for TiN; red, yellow, and orange mark is for HfO_2 with different orientations.

Interestingly, as the layer thickness decreased to 4 nm in the 45-layers film, Type I hyperbolic dispersion was observed, as shown in Figure 5c. When the wavelength is above 370 nm, $\epsilon^{\perp}$ is negative and $\epsilon^{//}$ shows positive. Such Type I hyperbolic dispersion was usually detected in the VAN structure, where metal pillars embedded in the dielectric matrix.[9,21,23,24] It suggests that the TiN/HfO_2 multilayer structure could be regarded as a dielectric unit when the layer thickness reduces to 4 nm in this 45-layers film, which is similar as a superlattice structure.[37] Such anisotropic structure, where Au pillars embedded in such dielectric unit, leads to the Type I hyperbolic dispersion. On the other side, the much stronger metallic expression in 45-layers film compared to 5-layers film can also result from the difference of HfO_2 layers. Since the HfO_2 layers were deposited by naturally oxidizing the TiN during the growth. In 45-layers film, there were more TiN layers, which can act as the oxygen barrier, and the obtained HfO_2 layer could be HfO_xN_y leading to a more metallic optical response.

As for the 15-layers film, a mixture property was identified. In the range from 475 to 550 nm, the Type II hyperbolic dispersion can be observed, where $\epsilon^{\perp}$ is positive and $\epsilon^{//}$ is negative. While the Type I hyperbolic dispersion can be observed above 725 nm. Comparing the fitted plot from 5-layers film and 15-layers film, it worth noticing that the value of $\epsilon^{\perp}$ turns to more negative as the wavelength increase in the 15-layers film, which indicating a more metallic behavior in the out-of-plane direction compared to the 5-layer film.

In addition, the imaginary part of the permittivity ϵ_2 was also plotted in Figure S3 (Supporting Information). It can be observed that the ϵ_2 along in-plane direction is similar for all three samples, but the ϵ_2 along out-of-plane direction, especially at optical and near-IR frequencies, is increasing as the layer thickness decreases. This can be resulted from the strong losses of TiN and Au components, and such a three-phase structure makes the optical response complicated. However, the imaginary part of the permittivity of all three samples are much lower than that of pure Au and TiN, indicating a lower absorption loss.[38]

To better understand such dispersion variation, the TiN/HfO_2 multilayer samples without Au pillars were also prepared with the same deposition parameters. The relative permittivity was measured and fitted, and the real part of the permittivity was plotted in Figure S5 (Supporting Information). It can be observed that 5 layers sample shows Type II hyperbolic dispersion which is commonly observed in dielectric/metal multilayer structure. However, as the layer thickness decreases, the TiN/HfO_2 multilayer structure becomes less anisotropic in 15 layers sample. As

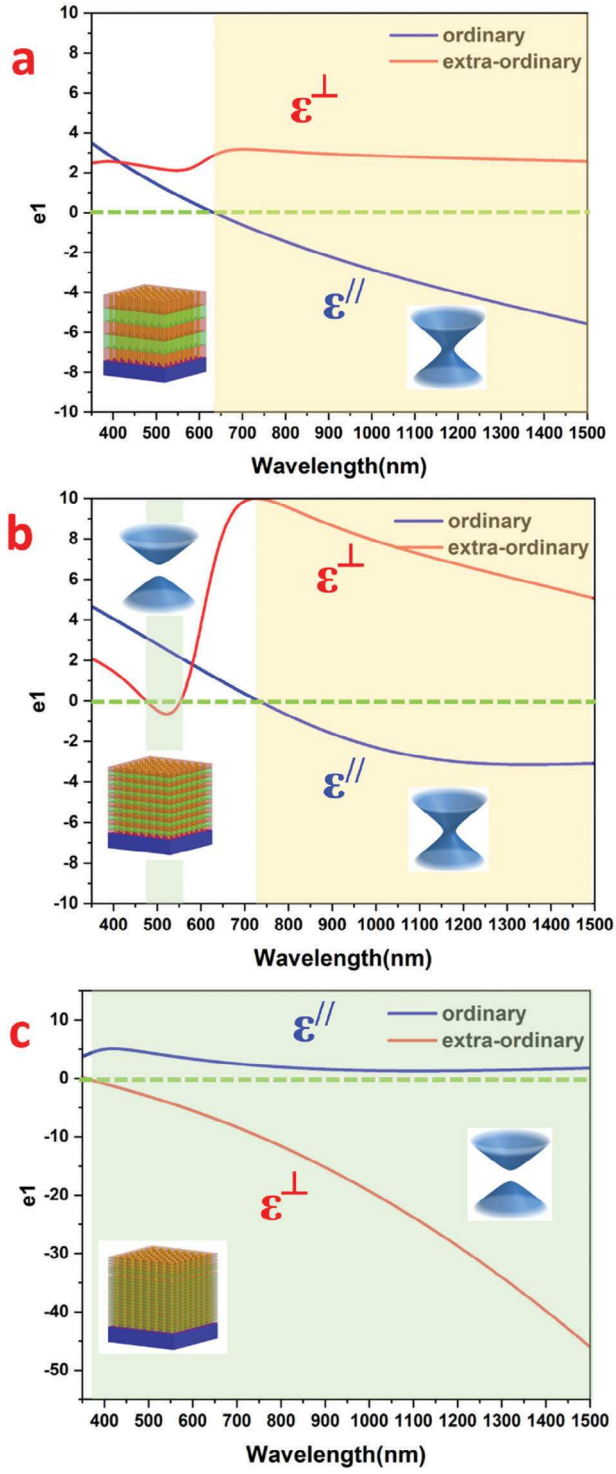

Figure 5. Dielectric constant e1 of HfO_2-Au/TiN-Au multilayer thin films with different numbers of layers: (a) 5 layers, (b) 15 layers, (c) 45 layers. Different hyperbolic dispersion was detected in different films following a certain trend.

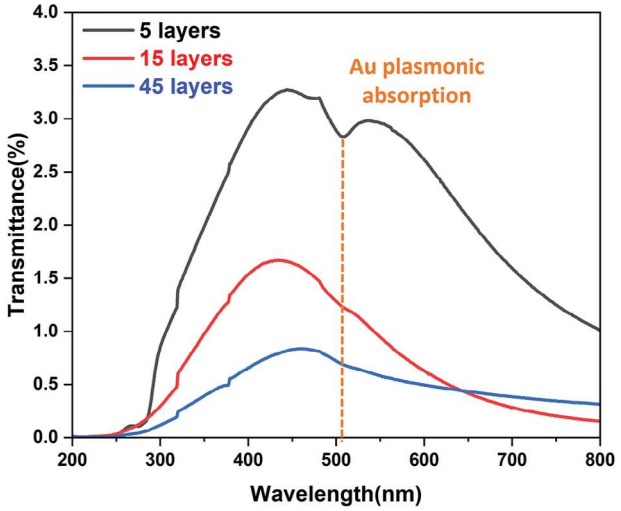

Figure 6. Transmittance of HfO_2-Au/TiN-Au multilayer thin films with different numbers of layers. Au plasmonic absorption peak was detected around the wavelength of 510 nm. (Some minor spectral features around wavelengths 320 nm, 380 nm, and 480 nm may result from the wavelength change of the machine during measurement.)

for the 45 layers TiN/HfO_2 sample, it shows both positive permittivity along in-plane and out-of-plane direction. This result agrees with our hypothesis that such TiN/HfO_2 multilayer structure can be regarded as a dielectric unit when the layer thickness reduce to a certain level. This can also help explain the hyperbolic dispersion transformation shown in Figure 5.

In addition, COMSOL simulation was conducted to help better understanding of the findings. A model with a 5-layer TiN/HfO_2 multilayer structure with or without Au was set in the simulation. The distribution of Au pillars was set based on the estimated volume fill fraction. The average diameter of Au pillar was set as 3.5 nm and the distance of Au pillars was set as 7 nm, then the volume fill fraction is set with the estimated value from microscope data, 20%. The simulated result is plotted in the Figure S6 (Supporting Information). It can be observed that the simulated plasmonic absorption peak is also ≈510 nm (mostly from the Au), which agrees well with the measured transmittance results. Since the actual interfaces of TiN and HfO_2 layers are not as ideal as that in the simulation, there is some shift and intensity difference between the simulated and measured transmittance data.

In short, the hyperbolic optical properties of this VAN and multilayers combined structure can be tuned by adjusting the layer thickness of each layer. When the layer thickness is large, the entire film behaves more as multilayers, which exhibits Type II hyperbolic dispersion. However, as the layer thickness decreases, the film behaves more as VAN, exhibiting Type I hyperbolic dispersion. This hybrid three-phase metamaterials with tunable hyperbolic property can be adopted for future hyperbolic optical device design.

Since Au is a typical plasmonic material, the plasmonic properties of the films were also investigated by transmittance measurement, and the results are shown in **Figure 6**. It can be observed that the transmittance curves of three samples follow a general trend, i.e. the intensity of the transmittance curves

decreases as the number of layers increases. This can result from the permittivity change of the samples. As shown in Figure 5, a higher layer number corresponds to a negative epsilon and hence no mode inside the material that can transport EM energy. In addition, the Au plasmonic absorption peak can be distinguished ≈510 nm in all three films. In addition, the Au plasmonic absorption peak can be distinguished ≈510 nm in all three films. Such short wavelength plasmonic absorption peak can be strongly affected by the morphology and background materials.[39,40] One possible reason can be size effect of the ultra-thin Au pillars embedded in the multilayers films, since the plasmonic absorption peak shows a redshift as the size increases.[41,42]

Overall, this study presents a multilayer-VAN combined metamaterial design with HfO_2-Au/TiN-Au multilayer thin films with fine Au nanopillars growing through the entire film, exhibiting tunable hyperbolic optical properties. A nitride/oxide/metal three-phase nanocomposite system with tunable optical property can offer a new design approach for future hyperbolic metamaterials.

3. Conclusion

In summary, self-assembled HfO_2-Au/TiN-Au multilayer thin films with thin Au nanopillars have been successfully obtained on MgO substrates by alternatively depositing HfO_2-Au and TiN-Au layers. The layer thickness of 20, 12, and 4 nm was carefully controlled by adjusting the laser pulses. One of the key considerations is to use HfN-Au to convert to HfO_2-Au VANs, instead of the direct HfO_2-Au deposition. This method minimizes the potential oxidation of TiN layer and thus maintains clean and sharp nitride/oxide interfaces in the multilayer samples. Such highly anisotropic nitride-oxide multilayer structure exhibits hyperbolic optical response. Interestingly, the type of hyperbolic dispersion can be tuned from Type II to Type I by reducing the layer thickness. Also, plasmonic absorption was observed near 510 nm.

It is noted that the crystallinity and epitaxial quality of the films were reduced as the layer thickness decreases. This could be due to the large lattice mismatch between the TiN layer and HfO_2 layers. For future directions, we can select other oxide and nitride systems with smaller lattice mismatch to achieve multilayer films with better crystallinity. It is also ideal to incorporate other metallic nanostructures for integrating other function properties into the multilayer-VAN combined hybrid metamaterials, such as magnetic nanocomposites, Co, Fe, and Ni nanopillars. With the large potential materials spaces and combinations, the property tuning could be broad and effective. Materials compatibility with the current IC fabrication process could also be another important consideration, for example, incorporating existing materials such as TiN, SiO_2, Cu, and others. This work offers a new approach for fabricating tunable hyperbolic metamaterials, which can be applied to future integrated photonic devices or sensor designs.

4. Experimental Section

Thin Film Growth: The multilayer-VAN combined thin films were deposited under vacuum using pulsed laser deposition (with a KrF excimer laser, $\lambda = 248$ nm). The multilayers thin film was fabricated with alternative layers of TiN-Au and HfO_2-Au on MgO substrates, where the bottom layer and top layer are always TiN-Au. The total deposition process was controlled to be 5000 pulses. The HfO_2-Au layer was deposited with an HfN-Au target. All the films with different layer thickness were deposited under vacuum at 600 °C.

Structure and Physical Properties Characterization: The microstructure of the films was characterized using X-ray diffraction (XRD) (PANalytical Empyrean, θ–2θ scan with CuKα radiation, $\lambda = 1.5406$ Å), Transmission Electron Microscopy (TEM), and Scanning Transmission Electron Microscopy (STEM), coupled with electron-dispersive X-ray spectroscopy (EDS). TEM, STEM, and EDS are all operated on ThermoFisher TALOS 200X under 200 kV accelerating voltage. The dielectric permittivity of the films was measured using a spectroscopic ellipsometer (JA Woollam RC2). The obtained data was modeled as in-plane ($\epsilon^{\parallel}$) and out-of-plane ($\epsilon^{\perp}$) components using the general oscillator models to make them Kramers–Kronig consistent. The transmittance of the films was measured using a Perkin Elmer Lambda 1050 system with a 3D detector.

Simulation: The numerical simulation was conducted with the COMSOL software. The relative dielectric data is from open source.

Supporting Information

Supporting Information is available from the Wiley Online Library or from the author.

Acknowledgements

This work was supported by the U.S. National Science Foundation DMR-2016453 (VAN thin film growth and High-resolution STEM work). J.S. acknowledges the support from the US Office of Naval Research (N00014-22-1-2600). The microscopy work was partially supported by the Lawrence Berkeley national laboratory (NCEM User Project). Lawrence Berkeley National Laboratory is a US DOE Office of Science national laboratory managed by the University of California. This paper describes objective technical results and analysis. Any subjective views or opinions that might be expressed in the paper do not necessarily represent the views of the US Department of Energy or the United States Government.

Conflict of Interest

The authors declare no conflict of interest.

Data Availability Statement

The data that support the findings of this study are available in the supplementary material of this article.

Keywords

anisotropy, metamaterials, multilayers, PLD, tunability, vertically aligned nanocomposites (VANs)

Received: January 17, 2024
Published online:

[1] A. J. Hoffman, L. Alekseyev, S. S. Howard, K. J. Franz, D. Wasserman, V. A. Podolskiy, E. E. Narimanov, D. L. Sivco, C. Gmachl, *Nat. Mater.* **2007**, *6*, 946.

[2] A. Fang, T. Koschny, C. Soukoulis, *Phys. Rev. B.* **2009**, *79*, 245127.
[3] K. Sreekanth, A. De Luca, G. Strangi, *Appl. Phys. Lett.* **2013**, *103*, 023107.
[4] J. Li, L. Fok, X. Yin, G. Bartal, X. Zhang, *Nat. Mater.* **2009**, *8*, 931.
[5] M. Otomori, T. Yamada, K. Izui, S. Nishiwaki, J. J. S. Andkjær, *Struct. Multidiscip. Optimi.* **2017**, *55*, 913.
[6] D. R. Smith, D. Schurig, J. J. Mock, P. Kolinko, P. Rye, *Appl. Phys. Lett.* **2004**, *84*, 2244.
[7] C. Shen, Y. Xie, N. Sui, W. Wang, S. A. Cummer, Y. Jing, *Phys. Rev. Lett.* **2015**, *115*, 254301.
[8] A. Poddubny, I. Iorsh, P. Belov, Y. Kivshar, *Nat. Photonics* **2013**, *7*, 948.
[9] P. Shekhar, J. Atkinson, Z. Jacob, *Nano Convergence.* **2014**, *1*, 1.
[10] J. Huang, D. Zhang, H. Wang, *Mater. Today Phys.* **2021**, *16*, 100316.
[11] J. N. Acharyya, D. N. Rao, M. Adnan, C. Raghavendar, R. Gangineni, G. Vijaya Prakash, *Adv. Mater. Interfaces* **2020**, *7*, 2000035.
[12] B. Saha, G. V. Naik, S. Saber, C. Akatay, E. A. Stach, V. M. Shalaev, A. Boltasseva, T. D. Sands, *Phys. Rev. B* **2014**, *90*, 125420.
[13] G. V. Naik, B. Saha, J. Liu, S. M. Saber, E. A. Stach, J. M. Irudayaraj, T. D. Sands, V. M. Shalaev, A. Boltasseva, *Proc. Natl. Acad. Sci.* **2014**, *111*, 7546.
[14] P. Huo, S. Zhang, Y. Liang, Y. Lu, T. Xu, *Adv. Opt. Mater.* **2019**, *7*, 1801616.
[15] E. Plum, V. Fedotov, A. Schwanecke, N. Zheludev, Y. Chen, *Appl. Phys. Lett.* **2007**, *90*.
[16] A. W. Clark, A. Glidle, D. R. Cumming, J. M. Cooper, *J. Am. Chem. Soc.* **2009**, *131*, 17615.
[17] I. Murataj, M. Channab, E. Cara, C. F. Pirri, L. Boarino, A. Angelini, F. Ferrarese Lupi, *Adv. Optical Mater.* **2021**, *9*, 2001933.
[18] S. O. Morgan, A. Muravitskaya, C. Lowe, A. M. Adawi, J.-S. Bouillard, T. S. Horozov, G. J. Stasiuk, D. M. Buzza, *Phys. Chem. Chem. Phys.* **2022**, *24*, 11000.
[19] J. A. Roberts, S.-J. Yu, P.-H. Ho, S. Schoeche, A. L. Falk, J. A. Fan, *Nano Lett.* **2019**, *19*, 3131.
[20] S. Vignolini, N. A. Yufa, P. S. Cunha, S. Guldin, I. Rushkin, M. Stefik, K. Hur, U. Wiesner, J. J. Baumberg, U. Steiner, *Adv. Mater.* **2012**, *24*, OP23.
[21] Y. Zhang, D. Zhang, J. Liu, P. Lu, J. Deitz, J. Shen, Z. He, X. Zhang, H. Wang, *Nanoscale* **2022**, *14*, 11979.
[22] D. Zhang, H. Wang, *Adv. Photonics Res.* **2021**, *2*, 2000174.
[23] Y. Zhang, J. Song, P. Lu, J. Deitz, D. Zhang, H. Dou, J. Shen, Z. Hu, X. Zhang, H. Wang, *Adv. Mater. Interfaces* **2023**, 2300150.
[24] W. Dickson, G. A. Wurtz, P. Evans, D. O'Connor, R. Atkinson, R. Pollard, A. V. Zayats, *Phys. Rev. B* **2007**, *76*, 115411.
[25] M. Y. Shalaginov, V. V. Vorobyov, J. Liu, M. Ferrera, A. V. Akimov, A. Lagutchev, A. N. Smolyaninov, V. V. Klimov, J. Irudayaraj, A. V. Kildishev, A. Boltasseva, *Laser Photonics Rev.* **2015**, *9*, 120.
[26] O. Kidwai, S. V. Zhukovsky, J. E. Sipe, *Phys. Rev.* **2012**, *85*, 053842.
[27] D. Zhang, P. Lu, S. Misra, A. Wissel, Z. He, Z. Qi, X. Gao, X. Sun, J. Liu, J. Lu, X. Zhang, *Adv. Optical Mater.* **2021**, *9*, 2001154.
[28] R. Zhang, T. Lin, S. Peng, J. Bi, S. Zhang, G. Su, J. Sun, J. Gao, H. Cao, Q. Zhang, L. Gu, *Nano Lett.* **2023**, *23*, 3879.
[29] K. Yatsugi, K. J. N. Nishikawa, *Nanotechnology* **2019**, *30*, 335705.
[30] D. Shah, H. Reddy, N. Kinsey, V. M. Shalaev, A. Boltasseva, *Adv. Optical Mater.* **2017**, *5*, 1700065.
[31] P. Patsalas, N. Kalfagiannis, S. J. M. Kassavetis, *Materials* **2015**, *8*, 3128.
[32] A. Glaser, S. Surnev, F. Netzer, N. Fateh, G. Fontalvo, C. Mitterer, *Surf. Sci.* **2007**, *601*, 1153.
[33] H.-Y. Chen, F.-H. Lu, *J. Vac. Sci. Technol. A* **2005**, *23*, 1006.
[34] D. Zhang, S. Misra, L. Li, X. Wang, J. Jian, P. Lu, X. Gao, X. Sun, Z. Qi, M. Kalaswad, X. Zhang, *Adv. Optical Mater.* **2020**, *8*, 1901359.
[35] J. Liu, X. Wang, X. Gao, H. Wang, J. Jian, J. Huang, X. Sun, Z. Qi, S. Misra, Z. He, H. Wang, *Appl. Mater. Today* **2020**, *21*, 100856.
[36] L. Li, L. Sun, J. S. Gomez-Diaz, N. L. Hogan, P. Lu, F. Khatkhatay, W. Zhang, J. Jian, J. Huang, Q. Su, M. Fan, *Nano Lett.* **2016**, *16*, 3936.
[37] J. L. MacManus-Driscoll, R. Wu, W. Li, *Mater. Horiz.* **2023**.
[38] J. Gosciniak, J. Justice, U. Khan, B. Corbett, *MRS Adv.* **2016**, *1*, 317.
[39] Q. Xu, J. Bao, F. Capasso, G. Whitesides, *Angew. Chem. Int. Ed.* **2006**, *45*, 3631.
[40] V. Amendola, R. Pilot, M. Frasconi, O. M. Maragò, M. A. Iatì, *J. Phys.: Condens. Matter* **2017**, *29*, 203002.
[41] J. Huang, T. Jin, S. Misra, H. Wang, Z. Qi, Y. Dai, X. Sun, L. Li, J. Okkema, H. T. Chen, P. T. Lin, *Adv. Optical Mater.* **2018**, *6*, 1800510.
[42] S. Link, M. A. El-Sayed, *J. Phys. Chem. B* **1999**, *103*, 4212.

